

# Bright Ångstrom and picometer free electron laser based on the Large Hadron electron Collider energy recovery linac

Z. Nergiz\*

*Nigde Omer Halisdemir University, Faculty of Arts and Sciences, Physics Department, 51200 Nigde, Turkey*

N.S. Mirian†

*Deutsches Elektronen-Synchrotron (DESY), 22607 Hamburg, Germany;  
and European Organization for Nuclear Research (CERN), 1211 Geneva 23, Switzerland*

A. Aksoy

*Ankara University, Institute of Accelerator Technologies, 06830, Ankara, Turkey;  
and Turkish Accelerator and Radiation Laboratory, 06830, Ankara, Turkey*

D. Zhou

*High Energy Accelerator Research Organization (KEK), Tsukuba, Ibaraki, Japan*

F. Zimmermann

*European Organization for Nuclear Research (CERN), 1211 Geneva 23, Switzerland*

H. Aksakal

*Kahraman Maras Sutcu Imam University, 46040 Kahramanmaras, Turkey*

The Large Hadron electron Collider (LHeC) is a proposed future particle-physics project colliding 60 GeV electrons from a six-pass recirculating energy-recovery linac (ERL) with 7 TeV protons stored in the LHC. The ERL technology allows for much higher beam current and, therefore, higher luminosity than a traditional linac. The high-current, high-energy electron beam can also be used to drive a free electron laser (FEL). In this study, we investigate the performance of an LHeC-based FEL, operated in the self-amplified spontaneous emission mode using electron beams after one or two turns, with beam energies of, e.g., 10, 20, 30 and 40 GeV, and aim at producing X-ray pulses at wavelengths ranging from 8 Å to 0.5 Å. In addition, we explore a possible path to use the 40 GeV electron beam for generating photon pulses at much lower wavelengths, down to a few picometer. We demonstrate that such ERL-based high-energy FEL would have the potential to provide orders of magnitude higher average brilliance at Å wavelengths than any other FEL either existing or proposed. It might also allow a pioneering step into the picometer wavelength regime.

## I. INTRODUCTION

The Large Hadron electron Collider (LHeC) [1] is a proposed future lepton-hadron collider at CERN, which would be realized by colliding protons circulating in one of the existing rings of the Large Hadron Collider (LHC) with a 60 GeV electron beam from a six-pass recirculating racetrack-shape energy-recovery linac (ERL). The electron beam consists of bunches of  $3 \times 10^9$  particles each, spaced by 25 ns like the proton bunches, with an average beam current of about 20 mA [2]. A recent design variant considers a lower electron beam energy of 50 GeV, accompanied by a possibly higher beam current of up to 50 mA [3].

The high-current ERL of the LHeC would also provide the opportunity for driving a Free Electron Laser (FEL) [4]. Indeed, ERL-based FELs already operated, and operate, successfully in the electron-energy range of 10 to 200 MeV, e.g. at BINP [5], JAEA [6] and JLAB [7]. Their parameters are compiled in Table

Table I: Parameters of some operating ERL-based FELs.

Facility	BINP	JAEA	JLAB
Beam energy [MeV]	20	17	120
Peak current [A]	3000	35	300
Average current [mA]	100	8	8
Photon wavelength [ $\mu\text{m}$ ]	40	22	1.6
Average FEL power [W]	500	1	10,000
Pulse duration [ps]	50	0.32	0.17

I. A superconducting ERL with a higher beam energy of 0.5–1.0 GeV was proposed to produce 13.5 nm radiation, at 5 kW average power [8]. Another proposal with 5 GeV beam energy aimed at generating X-rays at Å wavelengths [9]. All of these operating or proposed facilities featured, or feature, a significantly lower beam energy than the LHeC FEL. Most similar to the LHeC-based FEL would be a possible upgrade of the European XFEL also based on an ERL-type of operation, with 100% duty factor and an average brightness of  $1.64 \times 10^{25}$  photons/s/mm<sup>2</sup>/mrad<sup>2</sup>/0.1% bandwidth at 8.5 GeV beam energy [10].

Though the LHeC is designed for energy frontier electron-hadron scattering experiments at the LHC,

\*Electronic address: znergiz@ohu.edu.tr

†Electronic address: najmeh.mirian@desy.de

it is conceivable that the ERL program can be temporarily redefined, independently of electron-hadron operation, as, for example, during the decade in which the LHC may possibly be reconfigured to double its hadron beam energy within the High Energy LHC (HE-LHC) proposal [11], and during which no lepton-hadron collisions would take place.

In view of the performance expected from the LHeC-FEL (see Section VII C) also the construction of a dedicated ERL-based X-ray FEL user facility could, and perhaps should, be considered.

## II. ADAPTING THE LHeC

The ERL of LHeC is of racetrack shape. For the proposed collider operation, a 500 MeV electron bunch coming from the injector would be accelerated in each of two 10 GV superconducting linacs during three revolutions, after which it has obtained an energy of 60 GeV. Three additional revolutions, now with deceleration instead of acceleration, reconvert the energy stored in the beam back to radiofrequency (RF) energy [1]. The beam emittance and the energy spread of the particle beam increase with beam energy due to quantum fluctuations.

For the LHeC proper, the electron-beam emittance is not critical, since the proton-beam emittance is quite large. Incoherent synchrotron radiation significantly increases the normalized rms emittance during the arc passages at 40 and 50 GeV beam energy, by about  $7 \mu\text{m}$  [1, Table 7.14]. However, in order to obtain coherent X-rays at low wavelengths in FEL operation the beam emittance must be sufficiently small. Partly because of this emittance requirement, for the FEL operation, we choose the electron beam energy as 40 GeV or lower, depending on the X-ray wavelength desired, rather than 60 GeV. Figure 1 illustrates the LHeC ERL-FEL configuration.

The beam energy of 40 GeV can be attained after two passes through the two 10 GeV linacs, instead of the three passes of the standard LHeC operation. The subsequent deceleration would also happen during two additional passes. An energy of 20 GeV would already be achieved after a single pass through the two linacs, again followed by another pass of deceleration. Beam energies of 10 and 30 GeV are also readily obtained after one or two turns, with appropriate linac voltages and phasing.

At high beam energy, the incoherent synchrotron radiation in the arcs blows up the energy spread and the transverse emittance. At a beam energy of 40 GeV, the accumulated relative energy spread induced by quantum fluctuations in the third LHeC arc is  $5.3 \times 10^{-5}$  (2 MeV) [1, Table 7.13]. By contrast, at 20 GeV the additional energy spread due to incoherent synchrotron radiation (ISR) is negligible. For the chosen optics, the minimum additional contribution to the normalized emittance from incoherent synchrotron radiation is about  $0.5 \mu\text{m}$  at 40 GeV [1, Table 7.14], which is to be added to the initial emittance. At

20 GeV, the ISR effect, also on the transverse emittance, can be neglected. Instead, here, the transverse normalized emittance may be limited solely by the performance of the RF gun, and the total emittance could be as low as, or lower than,  $0.5 \mu\text{m}$  for a bunch charge of 0.5 nC (so-called PITZ scaling) [12].

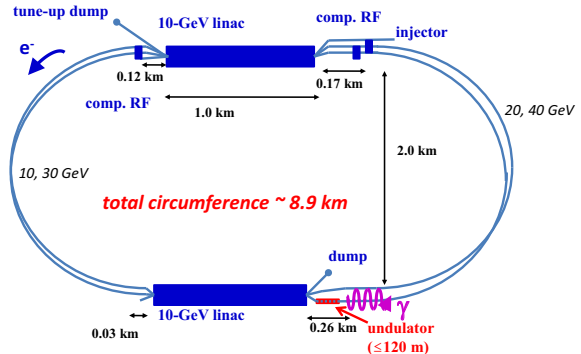


Figure 1: LHeC recirculating linac reconfigured for FEL operation.

## III. BUNCH COMPRESSION CONCEPT

Compared with chicane- or wiggler-based bunch compression in a single-pass linac [13–15], a recirculating linac offers additional degrees of freedom to compress the bunch and also to tailor its longitudinal profile, respectively, e.g. by exploiting the linear momentum compaction in the return arcs of the recirculating linac, and adjusting the RF phases for each linac pass. Additional manipulations would be possible by controlling (and cancelling) the second-order momentum compaction through arc sextupole magnets [16]. For example, choosing the proper linac configuration, in the downstream SLC (SLAC Linear Collider) arcs the rms bunch length could be compressed by more than an order of magnitude, from above 1 mm down to about  $50 \mu\text{m}$  [17].

To examine the possible LHeC ERL bunch-length compression for FEL operation, we accelerate the beam off-crest in some of the first three linac passages, and exploit the momentum dependent path length for the first three LHeC ERL arcs [1, 18], which for the CDR optics, including spreaders and combiners, amount to  $R_{56}^{(1)} = R_{56}^{(2)} = 0.21 \text{ m}$  and  $R_{56}^{(3)} = -0.31 \text{ m}$ , where the superindex in parentheses counts the arc, and a positive value for the fifth coordinate,  $z > 0$ , refers to a particle ahead of the synchronous particle.

However, the additional energy spread due to incoherent synchrotron radiation induced in the third arc  $\Delta\sigma_{\delta}^{(3)} \approx 5 \times 10^{-5}$ , along with the rather large (absolute) design value of  $|R_{56}^{(3)}| = 0.31 \text{ m}$ , contributes to the final bunch length a minimum amount of  $\Delta\sigma_{z,\text{min}} \geq |R_{56}^{(3)}| \Delta\sigma_{\delta}^{(3)} / \sqrt{3} \approx 9 \mu\text{m}$ , not yet including any nonlinear contributions. Hence, this optics does not allow squeezing the rms bunch length to val-

ues much below  $10 \mu\text{m}$ .

In view of this limit, and profiting from the flexible momentum compaction (FMC) arc optics, we have explored the possibility of changing the optics of arc 3, so as to be similar to those of arcs 1 and 2, or even further reducing the (absolute) value of  $R_{56}^{(3)}$ , allowing the compression to significantly shorter bunch lengths. The possibility to compress to shorter bunches, however, comes at the expense of a larger  $I_5$  radiation integral. Synchrotron radiation in arc 3 then increases the horizontal normalized emittance to total values well above  $2 \mu\text{m}$ . This emittance would be too large for the FEL wavelengths we are targeting.

We have, therefore, proceeded with the arc-3 optics from the LHeC CDR, which limits the possible compression to final rms bunch lengths not much below  $10 \mu\text{m}$ , but provides for a smaller transverse emittance, below  $1 \mu\text{m}$ .

In addition to the incoherent synchrotron radiation, also the effects of wake fields and coherent synchrotron radiation need to be taken into account.

#### IV. SHIELDED COHERENT RADIATION

The large bending radius of the LHeC,  $\rho \approx 750 \text{ m}$ , combined with a small vacuum chamber, suppresses the emission of synchrotron radiation at long wavelengths and, in particular, the emission of CSR [19, 20]. Specifically, synchrotron radiation is shielded at wavelengths longer than [21–23][24, Eq. (178)][25]

$$\lambda_{\text{sh}} \approx 2\sqrt{\frac{d^3}{\rho}}, \quad (1)$$

or, equivalently, for bunch lengths exceeding

$$\sigma_{z,\text{sh}} \approx \sqrt{\frac{d^3}{\rho\pi^2}}, \quad (2)$$

where  $d$  denotes the beam pipe diameter [23]. Considering the LHeC FEL, for  $\rho \approx 750 \text{ m}$  and  $d \approx 20 \text{ mm}$ , we find  $\sigma_{z,\text{sh}} \approx 30 \mu\text{m}$ . With a reduced pipe diameter of  $d \approx 10 \text{ mm}$ , we would expect to obtain complete CSR shielding down to  $\sigma_{z,\text{sh}} \leq 12 \mu\text{m}$ .

A few programs are available to simulate the shielding for a realistic closed vacuum chamber, rather than in free space or with parallel-plate boundaries. We employ the code CSRZ [25] to compute the CSR impedance in the frequency domain for an LHeC arc dipole of length  $4 \text{ m}$ , with a bending radius  $\rho \approx 750 \text{ m}$ . The shielding calculation considers a square vacuum chamber with variable curvature of the beam orbit. The CSR wake field can be calculated from the impedance by convolution with the spectrum of a given longitudinal bunch profile [26]. Figure 2 compares the CSR impedance of an LHeC arc dipole and the resulting wake function for a  $50 \mu\text{m}$  long bunch (blue curves) with those expected from a parallel-plate model, for a full aperture  $d$  of  $2 \text{ cm}$  (green curve). It

also illustrates the further dramatic reduction of the CSR impedance and wake field if the square chamber size is reduced to  $1 \text{ cm}$  (red curve). The maximum wave number  $k_{\text{max}}$  ( $k = \omega/c = 2\pi f/c$ ) corresponds to about  $5/\sigma_z$  with a typical  $50 \mu\text{m}$  rms bunch length in the third arc. Taking into account the bunch lengths in the different arcs (see Table II) for the first arc we choose a cutoff wave number  $k_{\text{max}}$  of  $30000 \text{ m}^{-1}$ , for the second arc  $60000 \text{ m}^{-1}$ , and for the last arc  $100000 \text{ m}^{-1}$ . In the tracking simulations performed with the code ELEGANT, at each dipole we include the CSR impedance, from CSRZ, corresponding to a full vertical and horizontal chamber aperture of  $1 \text{ cm}$ .

We neglect the possible interference between CSR wake fields from consecutive dipole magnets, but apply the CSR impedance independently in each dipole magnet, which, from past experience for other accelerators, represents a good first approximation.

We note that the suppression of both incoherent SR and CSR by the vacuum chamber has been well proven experimentally. For the SLC collider arcs, with  $d = 10 \text{ mm}$  and  $\rho = 280 \text{ m}$ , CSR should be shielded at  $\sigma_z > 20 \mu\text{m}$ , fully consistent with the complete absence of any CSR effects in the observed beam evolution for minimum bunch lengths around  $50 \mu\text{m}$  [17]. A later series of dedicated shielding studies at the BNL ATF further corroborated the theoretical predictions for CSR shielding [27]. Additional experimental evidence for the suppression of (in this case, incoherent) synchrotron radiation by the vacuum chamber, and for the predicted dependence on the bending radius, comes from RHIC, where fully stripped gold ion ( $\text{Au}^{+79}$ ) experienced a nearly total suppression of synchrotron radiation (energy loss per turn reduced by more than a factor ten) at an energy of  $70 \text{ GeV/nucleon}$ , and still a reduction by a factor larger than two at  $100 \text{ GeV/nucleon}$  [28]. These experimental results are consistent with CSRZ simulations.

#### V. WAKE FIELDS

The transverse and longitudinal wake fields in the LHeC linac RF cavities are modeled using the short-range wake functions of [29, Eq. (2.17)], which are based on Refs. [30, 31] (also see the illustration in [29, Fig. 2.2]). More precisely, the simulation uses the wake potentials (Green function wake fields), and then computes the bunch wake field from the actual particle distribution whenever the tracked bunch passes through a cavity. To illustrate the magnitude of the LHeC linac wake field, the nominal wake potential results in a longitudinal loss factor of  $2.6 \text{ V/pC}$  per cavity in case of a Gaussian bunch with  $2 \text{ mm}$  rms length.

Resistive-wall wake fields may set a lower limit on the acceptable vacuum chamber dimension in the arcs. The material of the LHeC vacuum chamber has not been decided. It could be made from copper or aluminum, and possibly be coated [1]. The characteristics of the resistive wall wake field is determined

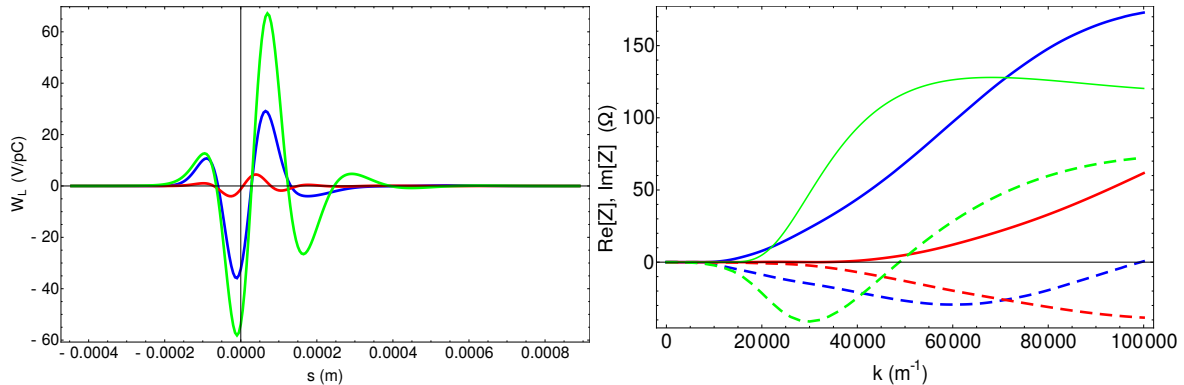


Figure 2: CSR wake field for a Gaussian bunch with 50 micron bunch length (left) and impedance (right) for a 4-m long arc dipole with  $\rho = 744$  m computed by the code CSRZ [25] for a square beam pipe with 2 cm (blue) or 1 cm full aperture (red) in the horizontal and vertical direction, compared with the CSR wake and impedance calculated for a simple parallel plate model with a vertical gap of 2 cm (green). In the right picture, solid lines refer to the real part, dashed lines to the imaginary part of the impedance.

by the parameter  $s_0 \equiv (d^2 \rho_{\text{res}} / (2Z_0))^{1/3}$  [32, 33], with  $Z_0$  the impedance of free space (about  $120\pi \Omega$ ). The wake function is approximately constant over distances much shorter than  $s_0$ , but it oscillates over distances of a few  $s_0$ . Assuming that the LHeC arc vacuum chamber is made from copper, with a resistivity of  $\rho_{\text{res}} = 1.7 \times 10^{-8} \Omega \text{ m}$ , for the smallest chamber aperture considered,  $d = 10$  mm, we obtain  $s_0 \approx 13 \mu\text{m}$ , and the LHeC FEL bunches extend over several times  $s_0$ . In this regime the average energy loss over a section of length  $L$  is well approximated by [33, 34]

$$\Delta E_{\text{r.w.}} \approx -\frac{Z_0 c L N_b e^2}{5\pi d^2} \left(\frac{s_0}{\sigma_z}\right)^{3/2}, \quad (3)$$

where  $N_b$  denotes the bunch population,  $\sigma_z$  the rms bunch length, and  $L$  the length of the section in question (e.g.  $L \approx 3$  km for one arc). Also using  $d = 10$  mm,  $\sigma_z = 100 \mu\text{m}$  and  $N_b = 3 \times 10^9$ , we find for the average energy loss in the first arc  $\Delta E_{\text{r.w.}} \approx 4.9$  MeV. The rms energy spread induced by the resistive wall wake field will be of similar magnitude as the average energy loss. The estimated value of  $\Delta E_{\text{r.w.}}$  is about twice as high as the average energy loss due to the RF cavity wake fields in one linac.

Another possible concern is the transverse resistive wall wake field. The single-bunch resistive wall jitter amplification when passing through one arc, can be estimated, by averaging over several betatron oscillation periods, as [35, 36]

$$G \equiv \beta_y \frac{\Delta y'}{\Delta y} \approx \beta_y \pi^2 \frac{N_b r_e}{\gamma \sigma_z} \frac{L}{d^3} \langle f_R \rangle \sqrt{\lambda \sigma_z}, \quad (4)$$

where  $r_e$  denotes the classical electron radius,  $L$  again the length of the section in question (e.g.  $L \approx 3$  km for one arc),  $\gamma$  the Lorentz factor, and  $\lambda = \rho_{\text{res}} / (120\pi \Omega)$ . At a beam energy of 10 GeV, assuming a copper beam pipe, and using  $\langle f_R \rangle = 0.82$ ,  $d = 10$  mm,  $\sigma_z = 100 \mu\text{m}$ ,  $N_b = 3 \times 10^9$  and  $\beta_{x,y} \approx 50$  m, we find  $G \approx 0.3$ , which appears acceptable.

## VI. BUNCH COMPRESSION SIMULATIONS

Realistic longitudinal tracking simulations of two full circulations (four linac passages and three arc traversals) are performed with the code ELEGANT [37], which can take into account not only the linear and nonlinear optics, but, optionally, also the longitudinal and transverse linac wake fields, incoherent synchrotron radiation, and in addition, with an external “impedance” file, the effect of the shielded coherent synchrotron radiation in the arc dipole magnets, as computed by CSRZ. We have included all of these effects. However, our tracking simulations did not consider the (material-dependent) resistive wall wake field in the arcs. The CSR “impedance” file was varied according to the local bunch length. Below we present results for the nominal linac wake fields. We have also performed some simulations with a factor of 5 larger linac wake fields (that is, five times larger wake potentials), yielding quite similar results.

For every case, we have optimized the RF phases in each linac to achieve highest peak current after the third (first) arc or fourth (second) linac passage, and adjusted the linac RF voltage to maintain the target beam energy of 10, 20, 30 or 40 GeV. As a result of this optimization process, at 40 GeV the RF voltage of linac 1 was reduced to 9.7 GV and the one of linac 2 raised to 11.4 GV, for all passages.

Figure 3 shows the result of the optimization for 20 GeV, obtained by tracking 100,000 particles in ELEGANT through the first arc and two linac passages. Figure 4 presents the result of the optimization at 40 GeV, again obtained by tracking 100,000 particles in ELEGANT now through three arcs and four linac passages. Tracking a larger number of 200,000 particles yielded nearly identical results. Figures 3 and 4 show the simulated beam distribution in longitudinal phase after each of the two or four linac passages, and superimpose the corresponding bunch current profiles, a few parameters of which are compiled in Table II.

Table III summarizes the optimized electron beam

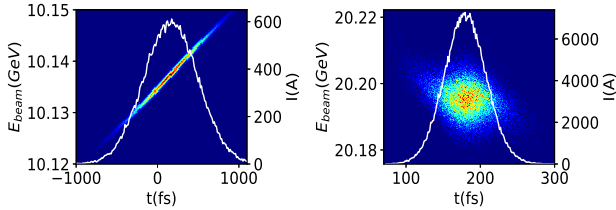


Figure 3: Beam distribution in longitudinal phase space after passing through linac 1 (left) and linac 2 (right) for 20 GeV FEL operation, obtained by tracking with ELEGANT [37], including the linac wake fields from Ref. [29], and the shielded CSR impedance from CSRZ [25]. The white dash-dotted line represents the current profile. The final FWHM bunch length is 63 fs, or 19  $\mu\text{m}$ , and the fitted rms bunch length  $\sigma_z = 8.5 \mu\text{m}$ .

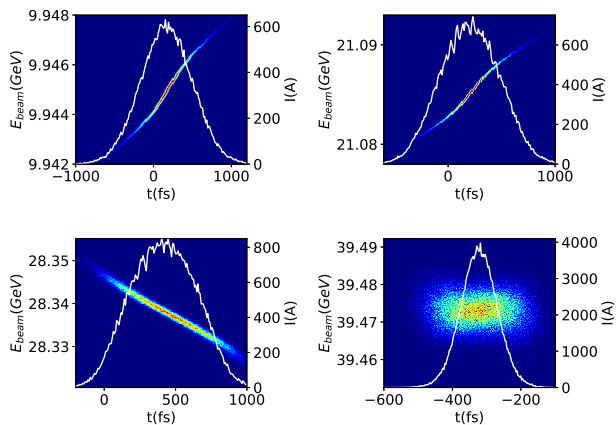


Figure 4: Beam distribution in longitudinal phase space after passing through linac 1 (top left) linac 2 (top right), linac 3 (bottom left) and linac 4 (bottom right) for 40 GeV FEL operation, obtained by tracking with ELEGANT [37], including the linac wake fields from Ref. [29], and the shielded CSR impedance from CSRZ [25].

parameters for LHeC FEL operation. The bunch compression using three linac passages and three arcs increases the peak bunch current by more than an order of magnitude while preserving a reasonable transverse emittance and energy spread suitable for FEL operation.

At 20 GeV, going through the first linac and the first arc, the bunch can be compressed by about a factor of 12 at the location of the undulator, from an initial rms length of 100  $\mu\text{m}$  down to an rms length of about 8  $\mu\text{m}$ ; see Fig. 3 and Table II. For a beam energy of 40 GeV, using three linac passages followed by three arcs, we achieve a bunch compression by about a factor of 9, down to an rms length of about 15  $\mu\text{m}$ , as is illustrated in Fig. 4.

For comparison, at LCLS II the rms bunch length can be varied between 0.6 and 52  $\mu\text{m}$ , with a nominal value of 8.3  $\mu\text{m}$  [38], and the nominal rms bunch length of the European X-FEL is 25  $\mu\text{m}$  [39].

The purpose of the present paper is to demonstrate

Table II: Parameters characterizing the longitudinal bunch profile for each linac passage: full-width-half-maximum (FWHM), FWHM divided by 2.355 (equal to a standard deviation  $\sigma$  for a Gaussian profile), the rms bunch length  $\sigma_z$  obtained from a Gaussian fit, and the peak current. The numbers in parentheses refer to the 20 GeV case.

Linac	FWHM [ $\mu\text{m}$ ]	FWHM/2.355 [ $\mu\text{m}$ ]	fitted $\sigma_z$ [ $\mu\text{m}$ ]	$\hat{I}_b$ [kA]
linac 1	228	97	100	0.6
linac 2	204 (19)	86.6 (8.3)	82.5 (8.5)	0.7 (7.3)
linac 3	175	75	66	0.8
linac 4	35	15	16	4

Table III: The main LHeC-ERL electron beam parameters. Peak current, bunch length, and transverse emittance were obtained from the tracking simulation. The numbers in parentheses refer to the 20 GeV case.

Parameters	Unit	Value
injection energy	GeV	0.5
final energy	GeV	40 (20)
electrons per bunch		$3 \times 10^9$
initial FWHM bunch length	$\mu\text{m}$	234
final FWHM bunch length	$\mu\text{m}$	35 (19)
initial peak beam current	kA	0.6
final peak beam current	kA	4 (7.2)
final hor. normalized emittance	$\mu\text{m}$	0.9 (0.4)
final vert. normalized emittance	$\mu\text{m}$	0.4
bunch spacing	ns	25
final rms energy spread	%	0.01

the capacity of the LHeC-ERL for high gain FEL operation. Precise beam dynamics simulation require separate, additional work, in particular detailed studies of the strong compression of electron bunches in the presence of both CSR and resistive wall wake fields.

Concerning the initial beam parameters, we note that for the 20 GeV simulations, where the compression is accomplished in the first arc, we considered an initial rms relative energy spread at 500 MeV of about  $10^{-3}$  ( $\sim 0.5$  MeV), as was also assumed in the LHeC design report [1, Section 7.3.3]. This energy spread proved sufficient to suppress the microbunching. In the case of 40 GeV simulations, we observed that microbunching does not occur even for a ten times lower initial relative rms energy spread at 500 MeV of  $10^{-4}$  (50 keV), since the incoherent synchrotron radiation in the second and third arc introduces a much larger rms spread of 0.4 and 1.6 MeV, respectively.

In our simulations, we have not included the resistive wall wake field directly. In the SLC arcs, with their compact aluminum vacuum chamber, not only the resistive wall, but also the wake fields of bellows and beam-position-monitors were significant [17]. To explore the sensitivity to wake fields in general, we have increased the magnitude of the linac wake fields

by up to a factor of 5. Always readjusting the linac RF phases, after bunch compression, we obtained a similar bunch length and the same, or even slightly higher, peak current as for the nominal linac wake fields. We expect that the same would be true for other wake fields that induce a correlated energy variation, of similar magnitude, along the length of the bunch. Instead of wake fields, it is the (random) energy spread introduced by the incoherent synchrotron radiation in the arcs which ultimately limits the achievable bunch length.

## VII. FEL CONSIDERATIONS

In a free-electron laser, the active medium is a beam of relativistic electrons. The FEL interaction amplifies the undulator radiation in the forward direction, leading to an exponential growth of the radiation power along the length of the undulator. A self-amplified spontaneous emission (SASE) FEL does not require any optical cavity, nor any coherent seed, and it can operate in the X-ray regime. The wavelength of the radiation is given by the well-known formula

$$\lambda = \frac{\lambda_u}{2\gamma^2} \left( 1 + \frac{K^2}{2} \right), \quad (5)$$

where  $\lambda_u$  denotes the period length of a (planar) undulator,  $\gamma$  the relativistic factor, proportional to the electron energy, and  $K$  the undulator parameter [40].

The optimum matching of the electron beam to the light beam is achieved under the diffraction limit condition

$$\varepsilon_N \leq \gamma \frac{\lambda}{4\pi}, \quad (6)$$

where  $\varepsilon_N \equiv \gamma\varepsilon$  signifies the normalized emittance. However, it has been demonstrated that FELs can still operate, albeit with a reduced efficiency, even if the normalized emittance exceeds this optimum condition by a factor of four to five [41]. Consequently, we expect that FEL light of wavelength around 0.5 Å can be produced by 40 GeV electrons with a normalized rms emittance of 0.9 μm.

The concrete goal of our LHeC ERL based FEL design is to generate hard X-ray FEL radiation in the range between about 0.5 Å and 8 Å. Following the second linac, we consider an FEL line featuring a planar undulator with 39 mm period length, similar to the soft X-ray undulator (SXU) line for LCLS II [42, 43]. The minimum gap of this kind of undulator is 7.2 mm, with a magnetic field at the minimum gap of 1.5 T, and a resulting undulator parameter  $K$  of 5.5. The planar undulator is characterized in Table IV. The targeted wavelength range can be covered by varying the electron beam energy from 10 to 40 GeV, in steps of 10 GeV, and changing the  $K$  value by opening the undulator gap.

With 40 GeV beam energy, tuning the undulator gap would actually also give us access to wavelengths

Table IV: Parameters of the planar undulator considered.

parameter	value
period length [mm]	39
number of periods	85
minimum gap [mm]	7.2
undulator parameter $K$	5.5
photon wavelength range [Å]	0.5–7.6

shorter than 0.5 Å. Besides, the LHeC ERL based FEL even offers opportunities to generate sub 10 pm FEL radiation. For this purpose, a second FEL line hosting a “Delta” undulator with 18 mm period [44] can be employed. However, obtaining and controlling the transverse coherence for the shorter wavelengths would benefit from a smaller transverse emittance of the 40 GeV electron beam (see Eq. (6)). Results of a preliminary study for a sub-10-pm FEL line are reported in Subsection VIII D.

### A. FEL Performance

Three-dimensional time-dependent simulations of the FEL process have been performed with the code GENESIS [45]. The electron beam energies considered — 10, 20, 30 and 40 GeV — correspond to photon wavelengths of about 7.6, 2.0, 1.0 and 0.5 Å, respectively. For the undulator beam line, a FODO lattice, with a half cell length of 4.095 m, was selected for its simplicity and cost-effectiveness, since it limits the total number of additional magnets. The length of each undulator is 3.315 m. Undulator modules are separated by intervals of 780 mm, providing some space for focusing, steering, diagnostics or vacuum-system components. Figure 5 shows the simulated power growth at different FEL wavelengths generated by electron beams of the corresponding energies. Depending on the wavelength the saturation occurs after a distance varying between 30 m and about 120 m. Figure 6 presents the spatial profile of the radiation pulses (first column), the spectrum of the radiation (second column), and the transverse cross section of the FEL radiation around the point of saturation, for beam energies of 10, 20, 30 and 40 GeV (from top to bottom).

### B. Undulator Wake Field

Longitudinal wake fields inside the undulator could increase the relative energy spread within the bunch, which for efficient lasing must stay less than a few times the Pierce parameter  $\rho$  [46, 47]. The dominant wake field inside the undulator is due to the resistive wall. Bane and Stupakov showed, for LCLS undulators, that taking into account the ac conductivity, a flat aluminum chamber is preferred over a round cop-

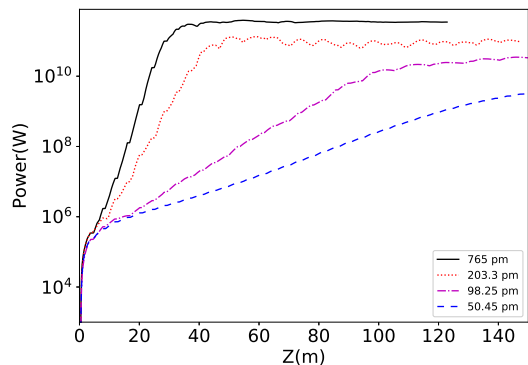


Figure 5: Growth of photon pulse power at 7.6 Å (black line) 2 Å (red dotted), 1 Å (magenta dot-dashed) and 0.5 Å (blue dashed) for an LHeC electron beam of energy 10, 20, 30 and 40 GeV, respectively, passing through the undulator FEL line with period  $\lambda_u = 39$  mm, as simulated with the code GENESIS.

per chamber, and that the anomalous skin effect can be neglected [48]. In this case the peak of the wake function has an amplitude of about  $Z_0 c / (a^2 c)$  where  $a$  denotes the vertical half gap [48],  $Z_0$  the vacuum impedance (about 377  $\Omega$ ), and  $c$  the speed of light. The effect of the wake field scales in first order with the bunch population  $N_b$ , and with the inverse of the beam energy  $E_b$ . For short bunches the wake field is independent of the bunch length, for long bunches it scales with the inverse 3/2 power; the transition between the two regimes occurs for bunch lengths of a few  $\mu\text{m}$  to tens of  $\mu\text{m}$  [32], depending on beam pipe radius and surface resistivity.

Compared with the LCLS, the LHeC FEL bunch lengths are roughly a factor 2 shorter (10  $\mu\text{m}$  versus 20  $\mu\text{m}$ ), but the bunch charge of the LHeC FEL is a factor 2 lower (0.5 nC versus 1 nC), the beam energy up to a factor 3 higher (40 GeV vs. 14 GeV). Combining these factors, for equal undulator length  $L_u$  and beam pipe radius ( $L_u \approx 130$  m, and  $a = 2.5$  mm for the LCLS [48]), the energy spread induced by the undulator wake field for the LHeC FEL should be less important than for the LCLS.

In addition, the average energy loss due to wake fields, arising along the length of undulator, could be partly compensated by tapering the field strength of the undulator as a function of longitudinal location.

The resistive-wall wake field does not only affect the beam, but it also leads to a significant heat load inside the undulator, which will need to be considered in an engineering design for the LHeC ERL-FEL.

### C. FEL Brilliance

One of the important parameters for comparing different radiation sources is the brilliance [49]. The brilliance describes the intensity of a light source including its spectral purity and opening angle. It

can be calculated from the spectral flux (in units of photons/s/0.1% bandwidth) by using the relation

$$B = \frac{\text{spectral flux}}{4\pi^2 \Sigma_x \Sigma'_x \Sigma_y \Sigma'_y}, \quad (7)$$

with the quantities

$$\Sigma = \sqrt{\sigma_e^2 + \sigma_{ph}^2} \quad (8)$$

and

$$\Sigma' = \sqrt{\sigma'_e{}^2 + \sigma'_{ph}{}^2}, \quad (9)$$

where  $\sigma_e$ ,  $\sigma'_e$ ,  $\sigma_{ph}$  and  $\sigma'_{ph}$  denote the transverse rms sizes and angular divergences of electron and photon beams [50]. In the case of full transverse coherence  $\Sigma \Sigma' = \lambda_{ph} / (4\pi)$ . The brilliance values for our four cases are listed in Table V, along with some other FEL parameters. A comparison of the LHeC ERL-FEL with a few existing and planned hard X-ray sources [38, 39, 41, 51, 52] is presented in Fig. 7. These figures demonstrate that the peak brilliance of the LHeC ERL-FEL is as high as the one of the European XFEL, while the average brilliance is orders of magnitude higher, thanks to the high average beam current, enabled by energy recovery.

The relatively high value of the horizontal emittance at 40 GeV causes a decrease in brilliance at wavelengths less than 1 Å. We note that the estimate of the LHeC ERL-FEL brilliance in this region is approximate, as the radiation is no longer fully coherent.

Table V: LHeC ERL-FEL radiation parameters derived from GENESIS simulations. The unit for the corresponding peak and average brilliance (B) is equal to photons/mm<sup>2</sup>/mrad<sup>2</sup>/s/0.1%bw.

electron energy (GeV)	10	20	30	40
wavelength (Å)	7.6	2.0	1	0.50
photon energy (keV)	1.63	6.2	12.4	24.8
saturation length (m)	30	40	100	120
peak power (GW)	70	18	5	1.7
pulse duration (fs)	60	60	120	120
bandwidth (%)	0.1	0.06	0.04	0.04
photons per pulse ( $\# \times 10^{10}$ )	1600	360	150	50
peak brilliance ( $B \times 10^{32}$ )	18	100	120	150
average brilliance ( $B \times 10^{27}$ )	4	25	65	70

Since the LHeC energy recovery linac provides a high-current, high-energy and high repetition rate electron beam, the average brilliance of the LHeC-FEL is greater, by at least three orders of magnitude, than for any other FEL source in operation or under construction in the world. It also is about two orders of magnitude higher than the projected average brightness predicted for ERL-extensions of presently existing X-ray FEL infrastructures, as, e.g., in Ref. [10]. Handling this bright a photon beam will

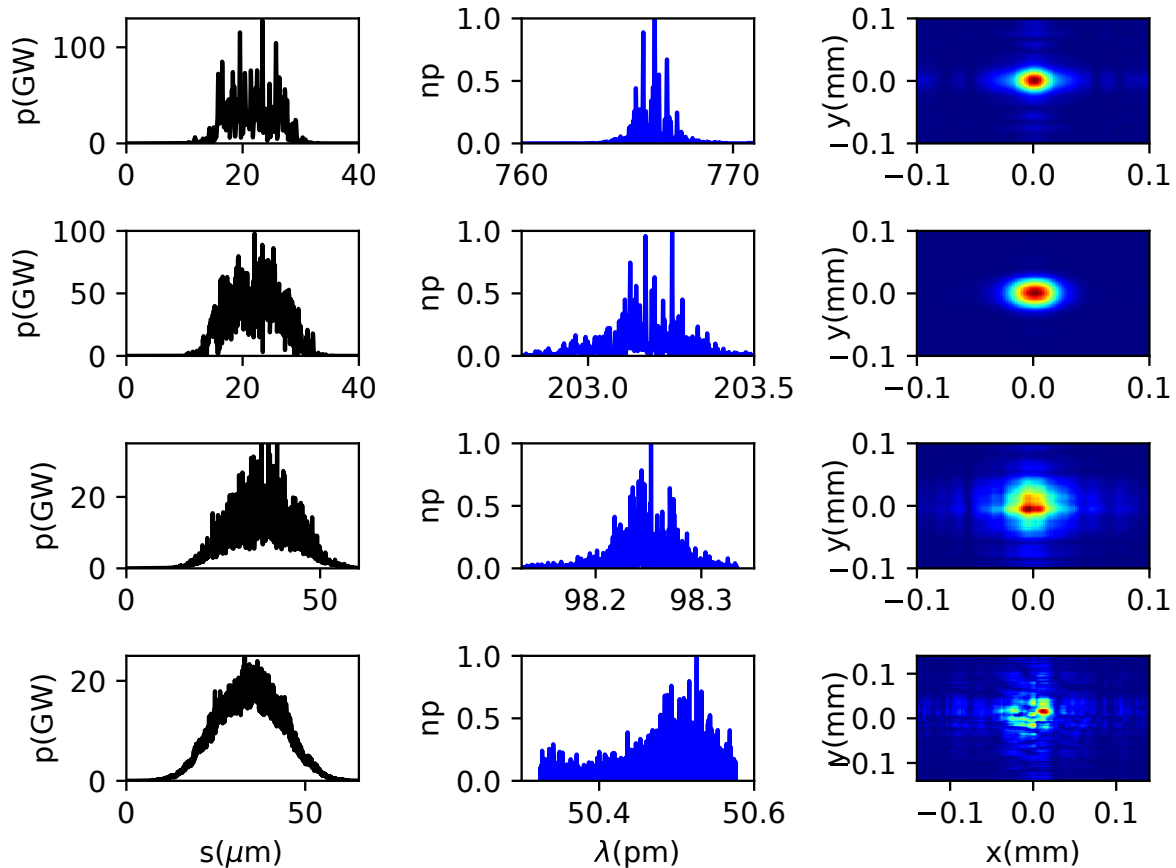


Figure 6: Spatial profile of the radiation pulse (left), wavelength spectrum of the radiation (centre) and transverse cross section of the of FEL radiation pulse around the point of saturation (right) for a beam energy of 10, 20, 30 and 40 GeV (from top to bottom), as simulated with GENESIS, using the respective distribution of the accelerated beam, obtained from ELEGANT, as input.

be challenging; it is likely that during the commissioning of the proposed facility the average beam current can only be raised slowly, as various technical obstacles might be encountered and need to be addressed.

#### D. Picometer FEL Radiation

To set foot in the domain of even shorter wavelengths, that is the sub-10-pm region, we need to deploy an undulator with shorter period length. For this purpose, we consider a “Delta undulator” with 18 mm period and 5 mm minimum gap. The Delta undulator [9, 44] is one of the best undulator sources for shaping the FEL photon polarization, and an example is currently employed at LCLS I. This type of undulator was originally proposed by A. Temnykh, who designed, built and tested a prototype Delta undulator with 24 mm period at Cornell University [44]. After this, Bilderback et al. proposed a Delta undulator with 18 mm period and 5 mm minimum gap for an ERL-based coherent hard X-ray source [9].

Our motivation for using this type of undulator source at the LHeC FEL is the prospect of producing radiation at wavelengths shorter than  $0.07 \text{ \AA}$  (7 pm) with a 30–40 GeV electron beam. Figure 8 illus-

trates the  $K$  parameter and the radiation wavelength of a 40 GeV electron beam as a function of the gap size, for both planar and helical operation mode of the Delta undulator, as obtained by applying Eq. (1) of Ref. [44]. Green (blue) dashed and solid lines show the  $K$  value (linked to the radiation wavelength) for the helical and planar Delta undulator, respectively.

Figure 9 presents our GENESIS simulations for the Delta undulator FEL line. The helical set up of the Delta undulator produces helical polarization, the planar set up linear polarization. The simulations at 6 pm wavelength were performed for a 30 GeV electron beam passing through the Delta undulator, with a gap of  $\sim 6.5$  mm, considering either helical or linear polarization, shown by the black solid and dashed line, respectively. The figure also presents the growth at radiation wavelengths of 4 and 2 pm, represented by the red and blue lines, for a 40 GeV beam passing through the helical or planar Delta undulator line.

Although both quantum fluctuations and slippage effects are included in these simulations, GENESIS simulations for wavelengths shorter than 10 pm may not be fully reliable. The reason is that GENESIS calculates the initial bunching factor from the number of macro-particles ( $N_{\text{part}}$ ) found over the distance of one wavelength, which, due to shot noise, would be



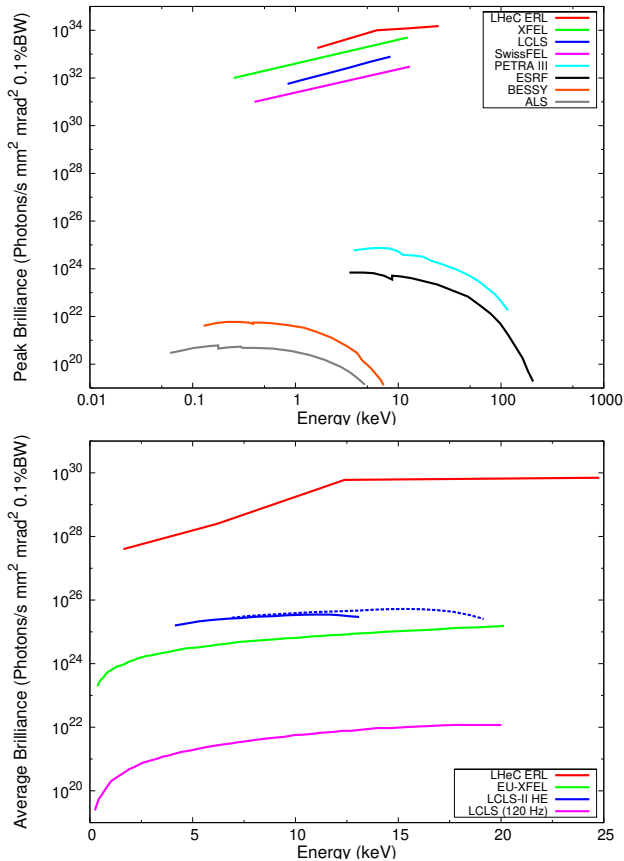


Figure 7: Comparison of FEL peak and average brilliance for the LHeC-FEL with several existing or planned hard X-ray FEL and SR sources [53].

$\langle b \rangle = 1/\sqrt{N_{\text{part}}}$ , and calculates the radiation power from this bunching factor. At longer wavelengths, the macro-particle number is usually less or equal to the actual number of electrons in one “beamlet” (i.e., found over the distance of one wavelength). For radiation wavelengths shorter than 10 pm, and with 4 kA peak current, the actual number of electrons in one beamlet is only a few hundred electrons. If the number of macro-particles inside a beamlet is lower, the GENESIS simulations may not reveal the correct sensitivity to the transverse profile. Conversely, if this number of macro-particles is higher than the actual number of electrons in a beamlet, the shot noise and bunching factor will be lower than in reality.

In view of these considerations, and to validate our simulation results, we have benchmarked them against estimates from 1D and 3D FEL theory. The FEL gain length in 1D is  $L_{G0} = \lambda_w / (4\pi\rho_{1D})$ , with  $\rho_{1D} \approx 1.4 \times 10^{-4}$  denoting the 1D FEL parameter [54], evaluated for a wavelength of 4 pm. Therefore, the one dimensional gain length for the helical Delta undulator is around 6 m, and the FEL power in saturation ( $P_{\text{sat}} = \gamma mc^2 I / \rho_{1D}$ ) is approximately 22 GW.

Taking into account the 3D effect on the FEL performance according to the methodology of E. Saldin et al. [55, Eqs. (3)–(5)], the 3D gain length at 4 pm wavelength increases to around  $L_{G,3D}^{E,S} = 17$  m. The gain

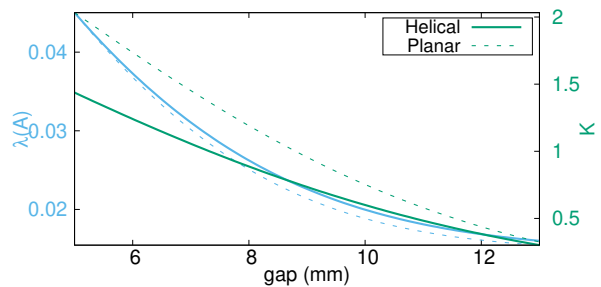


Figure 8: Radiation wavelength (left axis, blue) and  $K$  value (right axis, green) for a 40 GeV electron beam passing through the Delta undulator as a function of the gap of undulator, in case of helical (solid lines) or planar mode of operation (dashed lines). The period length of the undulator is taken to be 18 mm.

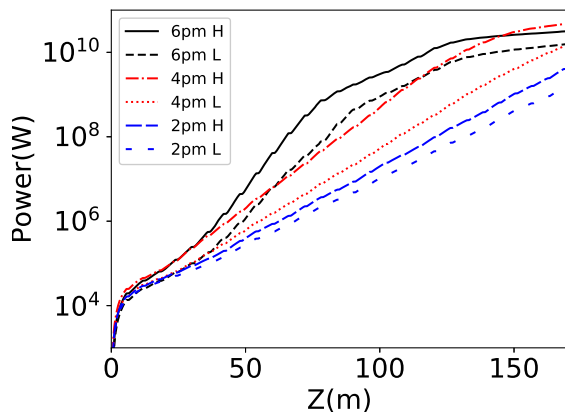


Figure 9: Simulated power growth for cases of helical (H) and linear (L) polarization of sub 10 pm radiation wavelengths. The simulations were performed for an electron beam of either 30 GeV (black lines) or 40 GeV (red and blue lines) passing through a helical or planar Delta undulator FEL line.

length in our simulation is almost 20 m (see Fig. 9). Accordingly, the results of our GENESIS simulations are not far from the 3D FEL theory of Ref. [55]. We can also consider another analytical model for the 3D FEL effect, namely the one of M. Xie [56]. According to Xie’s analysis, assuming an electron beam well matched to the design optics, the 3D power gain length, as a function of the average betatron function in the undulator, is calculated as  $L_{G,3D}^{M,X} = L_G(1 + \Lambda)$ , where  $\Lambda$  includes the effects of the radiation diffraction, the electron beam transverse emittance and the uncorrelated energy spread [56]. By using the values for our beam, the Xie formalism predicts  $\sim 22$  m gain length, which is again quite close to our simulation result. From these comparisons, we conclude that the GENESIS simulation results for wavelengths of a few

pm, presented in Fig. 9, are in good agreement with FEL theory.

Another issue of potential concern is that, in simulations with unprecedentedly high values of the photon energy, the recoil effect on the emitting beam particle may become important. At the wavelengths where this happens GENESIS will no longer produce correct results. The importance of the recoil is indicated by the quantum FEL parameter  $\bar{\rho}$ , defined as  $\bar{\rho} = \rho\gamma mc/(\hbar k)$ , which represents the ratio between the classical maximum induced momentum spread and the one-photon recoil momentum [57, 58]. If  $\bar{\rho} \leq 1$ , the FEL will exhibit a strong quantum recoil effect. Calculating the quantum FEL parameter at 2 pm wavelength (considering the helical Delta undulator with  $K=0.65$ ), we find  $\bar{\rho} \approx 5.9$ , which is larger than 1. The resulting quantum recoil parameter  $1/\bar{\rho}$  is 0.17. These numbers indicate that even at a wavelength of 2 pm the LHeC FEL dynamics remains essentially classical and is not strongly altered by the quantum recoil momentum. We note that, although the photon energy is high, the beam energy is much higher still, which explains the weak quantum recoil effect despite the short wavelength. In this case, the value of  $\bar{\rho}$  indicates the number of resonant photons emitted per electron at saturation [58].

In consequence, the simulations of Fig. 9 inspire confidence that the LHeC FEL can produce more than 1 GW FEL peak power at wavelengths shorter than 10 pm. This mode of operation in the pm wavelength regime could be another outstanding feature of the proposed new facility. We can even consider the higher harmonics of these few pm radiation lines. Specifically, it is well known that the higher harmonics of the radiation in helical undulators contain higher orders of the angular momentum  $\ell = (h - 1)$  [59, 60], where  $h$  denotes the number of the harmonic. Certainly, this ability can open a new pathway for studies of nuclear interactions.

In future studies of the short wavelength FEL operation based on the LHeC-ERL we may investigate various possibilities to further enhance the efficiency of this facility in the few pm wavelength regime, and to advance the FEL performance for wavelengths shorter than 50 pm, with the particular aim of improving the transverse coherence. One idea would be to reduce the electron bunch charge, so as to be able to inject a beam with lower initial emittance, and, in addition, to better control the transverse emittance growth due to synchrotron radiation by further optimizing the optics in the ERL arcs.

## VIII. ENERGY RECOVERY

The high average brilliance is achieved thanks to the high average beam current, which relies on energy recovery. For the energy recovery process, the energy spread of the electron beam after the lasing process is an important parameter. The evolution of this parameter is shown in Fig. 10 for an FEL wavelength

of 0.5 Å. Along the undulator, the relative energy spread increases approximately six times (from 0.01% to 0.06%), but it remains small compared with the energy acceptance of the optics. The energy spread at the saturation point ( $z \approx 120$ –150 m) is approximately 25 MeV. This value is low compared with the electron beam energy, and also with the electron injection energy of 500 MeV. It can further be reduced by energy compression in the downstream arcs and linacs.

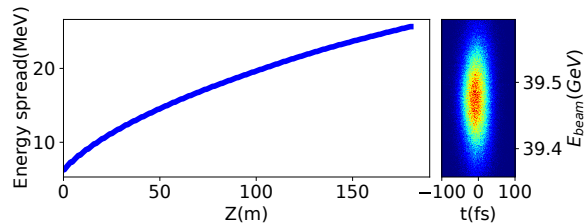


Figure 10: (Left) The evolution of beam energy spread ( $\sigma_E$ ) along the undulator region for 0.5 Å via 40 GeV e-beam energy through planar undulator. (Right) Longitudinal phase-space of e-beam after FEL radiation at 0.5 Å.

To study this aspect further and to demonstrate the feasibility of energy recovery during FEL operation, we have simulated the deceleration process from the maximum beam energy about 40 GeV down to about 0.5 GeV, starting with the beam distribution exiting the undulator, shown in Fig. 10. This distribution, modelled by  $8 \times 10^5$  macroparticles representing a single bunch, was obtained from the GENESIS FEL simulation for the 0.5 Å case. We next used again the simulation code ELEGANT to track the  $3 \times 10^5$  macroparticles through the exact optics [1, 18] for the last two decelerating turns (four arcs and four linac passages) of the LHeC, composed of 16,000 beam-line elements. As before for the acceleration, also here both the linac wake fields and the shielded CSR in the arcs were taken into account. To control energy spread and bunch length during deceleration the bunch arrival phase in the linacs was set to  $-170^\circ$  instead of the  $-180^\circ$  which would correspond to maximum deceleration. Figure 11 shows the simulated beam size, bunch length and beam energy during the deceleration process. In the simulation, not a single macroparticle was lost. The final rms beam of order 1 mm, is much smaller than the linac RF cavity iris radius of 7 cm [31]. We have verified that deceleration is also possible, and even easier, for the 20 GeV single-turn ERL operation.

## IX. APPLICATIONS FOR AN EXTREMELY BRILLIANT COHERENT X-RAY SOURCE

The brilliant photon beams at wavelengths below 1 Å generated by the LHeC FEL could potentially revolutionize scientific experiments in different fields of research such as biology, chemistry, material science, atomic physics, nuclear physics, and particle physics.

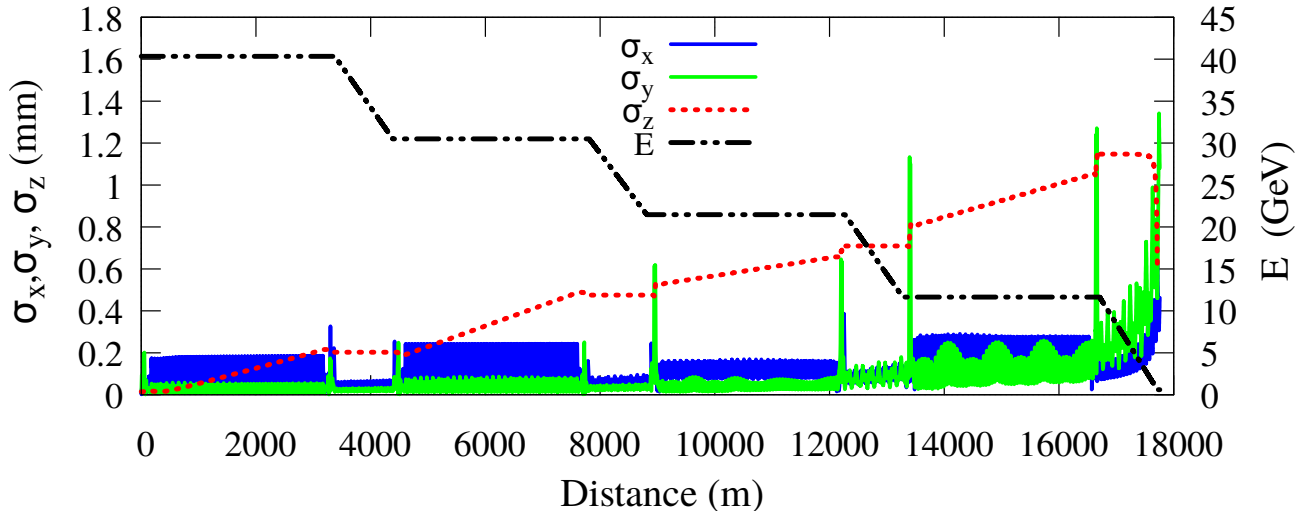


Figure 11: Beam energy and beta functions for the deceleration of the spent beam, after lasing at  $0.5 \text{ \AA}$ , over two complete LHeC turns starting from 40 GeV.

High-resolution high-brilliance X-rays, with wavelengths of less than  $1 \text{ \AA}$  would allow advanced imaging of enzymes [61], viral assemblies [62], and corona viruses [63], and, e.g., enable more efficient antiviral drug design [63]. Shorter wavelength dramatically improves atomic resolution data (e.g. approximately five times more data are expected to be available at  $0.95 \text{ \AA}$  resolution than at  $1.5 \text{ \AA}$  resolution [61]).

Hard X-rays with photon energies exceeding 10 keV ( $\lambda < 1.2 \text{ \AA}$ ) also enable studies of thick 3D materials due to their deep penetration paired with excellent spatial resolution. Such X-ray radiation allows probing condensed matter systems on the atomic length scale with minimum unwanted absorption.

One of the possible applications of LHeC FEL would be resonant inelastic X-ray scattering (RIXS) experiments. RIXS offers the unique capability to record excitation spectra from complex materials by measuring the momentum and energy dependence of inelastically scattered photons [64]. The cross section for RIXS scattering is extremely small compared with other techniques such as elastic X-ray scattering or X-ray emission spectroscopy. Therefore, the RIXS experiments require a high average brilliance [65].

Other “photon-hungry” experiments, which would be enabled by the LHeC/ERL-based FEL include total X-ray scattering, X-ray diffraction under high pressure, and resonant X-ray emission spectroscopy (RXES) [66]. RXES is a powerful method for studying the electronic structure of atoms, molecules and solid materials. The RXES signals are much weaker than those of X-ray absorption spectroscopy (XAS), so that, similar to RIXS, also RXES precision experiments require a high-brilliance X-ray source [67].

As a concrete example, studies of nano-materials for advanced battery technologies could greatly benefit from the high average brilliance available at the LHeC-FEL [68].

In general, the high average brilliance of the LHeC-

FEL will facilitate the detection of ultrafast changes of structures and of the electronic states of natural and artificial materials [69].

In addition, the proposed picometer FEL may prove a unique source of high-energy photons carrying orbital angular momentum, as an alternative to the proposed inverse Compton scattering of twisted laser photons off a relativistic electron beam [70].

Finally, in the area of particle physics, the unique average intensity and the wide photon-energy range of the LHeC FEL radiation could enable intriguing hunts for New Physics [71], including searches for Dark Photons and Axion-like Particles (ALPs) [72, 73].

## X. CONCLUSIONS

We have investigated the potential radiation properties of a SASE FEL based on an Energy Recovery linac, such as the LHeC. Our simulations of the FEL process, for LHeC electron beams of 10, 20, 30 and 40 GeV passing through a planar LCLS-II type undulator with 39 mm period, suggest that FEL radiation in the few Angstrom or sub-Angstrom wavelength regime can be produced, at significant power and brilliance (see Table V). Indeed, the LHeC-FEL promises an average brilliance far exceeding those of other, existing or proposed X-ray FELs.

In addition to using a high-energy, cw electron beam with 25 ns bunch spacing, the high average brilliance relies on the following two features. First, coherent synchrotron radiation is expected to be almost completely suppressed by realistic vacuum-chamber shielding, thanks to the large bending radius and small vacuum chamber of the LHeC machine. This assumption has been validated by detailed simulations using the codes CSRZ and ELEGANT. We note that these simulations did not take into account any resistive-wall wake fields, the magnitude of which was only es-

timated analytically. Second, we have shown that the beam exiting the undulator can be decelerated efficiently from 40 GeV down to a few 100 MeV, without any noticeable beam loss, which is the key prerequisite for the energy recovery mode of FEL operation.

The reported simulation results were obtained for the SASE FEL mode and without any tapering. By using self seeding and a tapered undulator the performance could be further improved and the spectrum be rendered more monochromatic. Furthermore, in combination with a low-loss crystal cavity, a free-electron laser oscillator operating in the Ångstrom wavelength regime could be realized [74].

We have also performed exploratory studies with a Delta undulator of 18 mm period, that could allow access to the extremely short wavelength range below 10 pm, using the 40 GeV electron beam of the LHeC.

In summary, an ERL-based high-energy SASE FEL boasts various unique characteristics and offers tantalizing opportunities. The advent of such a facility would impact numerous areas of fundamental and applied science.

## Acknowledgments

We thank Herwig Schopper, the Chair of the LHeC International Advisory Committee, for hinting at the use of the LHeC as an FEL. Particular thanks go to Sven Reiche from PSI, and to Gianluca Geloni and Svitozar Serkez from the European XFEL, for enlightening discussions on GENESIS simulations and effects at very short wavelengths. We are grateful to Alex Bogacz from Jefferson Lab for providing the LHeC optics files in MAD-X [75] format, which we converted to ELEGANT [37]. We also acknowledge continued encouragement from Oliver Brüning and Max Klein.

This work was supported by the Turkish Atomic Energy Agency with Grant No. 2015 TAEK (CERN) A5.H6.F2-13, and by the European Commission under the HORIZON2020 Integrating Activity project ARIES, grant agreement 730871.

- 
- [1] J.L.A. Fernandez et al., *Journal of Physics G: Nuclear and Particle Physics* **39**, 075001 (2012).
- [2] F. Zimmermann, O. Brüning, and M. Klein, *Proc. 4th International Particle Accelerator Conference*, Shanghai, China, 12 - 17 May 2013 p. 1017 (2013), URL <http://cds.cern.ch/record/1575158>.
- [3] P. Agostini et al., *The large hadron-electron collider at the hl-lhc* (2020), 2007.14491.
- [4] H. Schopper, Suggestion during the 2017 LHeC/FCC-eh Workshop (2017), <https://indico.cern.ch/event/639067>.
- [5] N.A. Vinokurov et al., *Proc. IPAC'17*, Copenhagen, Denmark p. 4836 (2017).
- [6] N. Nishimori et al., *Proc. FEL 2006*, BESSY, Berlin p. 265 (2006).
- [7] S. Benson et al., *Proc. PAC07*, Albuquerque, New Mexico p. 79 (2007).
- [8] Y. Socol et al., *Phys. Rev. ST Accel. Beams* **14**, 040702 (2011).
- [9] D. H. Bilderback, J. D. Brock, D. S. Dale, K. D. Finkelstein, M. A. Pfeifer, and S. M. Gruner, *New Journal of Physics* **12**, 035011 (2010), URL <https://doi.org/10.1088%2F1367-2630%2F12%2F3%2F035011>.
- [10] J. Sekutowicz et al., *Phys. Rev. ST Accel. Beams* **8**, 010701 (2005).
- [11] J.L. Abelleira et al., *J. Phys.: Conf. Ser.* **1067**, 022009 (2018).
- [12] B. Carlsten (2013), *Space Charge 2013 Workshop*, CERN, 18 April 2013.
- [13] S. Kheifets, R.D. Ruth, T.H. Fieguth, *Particle Accelerators* **30**, 79 (1990).
- [14] T.O. Raubenheimer, P. Emma, S. Kheifets, *Proc. IEEE PAC1993*, San Francisco p. 635 (1993).
- [15] P. Emma, T.O. Raubenheimer, F. Zimmermann, *Proc. IEEE PAC1995*, Dallas p. 704 (1995).
- [16] T. Kamitani et al., *Proc. APAC1998*, Tsukuba (1998).
- [17] K.L.F. Bane, P. Emma, M.G. Minty, F. Zimmermann, *Proc. 1st Asian Particle Accelerator Conference (APAC 98)*, Tsukuba, Japan (1998).
- [18] A. Bogacz, *Accelerator Seminar*, CERN and JLAB, 7 and 14 October 2010 (2010), URL [https://cds.cern.ch/record/1319025/files/LHeC\\_Recirculator\\_Bogacz.pdf](https://cds.cern.ch/record/1319025/files/LHeC_Recirculator_Bogacz.pdf).
- [19] J. Schwinger, *LBNL Report LBNL-39088* (1945).
- [20] J.S. Nodvick and D.S. Saxon, *Phys. Rev* **96**, 180 (1954).
- [21] A. Faltens and L.J. Laslett, *Part. Accel.* **4** (1973).
- [22] R.L. Warnock and P. Morton, *Part. Accel.* **25**, 113 (1990).
- [23] R.L. Warnock, *SLAC Report SLAC-PUB-5375* (1990).
- [24] T. Agoh, *Phys. Rev. ST Accel. Beams* **12**, 094402 (2009), URL <https://link.aps.org/doi/10.1103/PhysRevSTAB.12.094402>.
- [25] D. Zhou et al., *Jpn. J. Appl. Phys* **51**, 016401 (2012).
- [26] D. Zhou, *Conf. Proc. C* **1205201**, 52 (2012).
- [27] V. Yakimenko et al., *Phys. Rev. Lett.* **109**, 164802 (2012).
- [28] N.P. Abreu et al., *Proc. EPAC'08*, Genoa, Italy (2008).
- [29] D. Pellegrini, Ph.D. thesis, CERN (2016), 8 Apr 2016, URL <http://cds.cern.ch/record/2235763>.
- [30] K. L. F. Bane, *SLAC-PUB-9663*, LCC-0116 (2003).
- [31] R. Calaga, *CERN-ACC-NOTE-2015-0015* (2015), URL <http://cds.cern.ch/record/2020926>.
- [32] A. W. Chao, *Physics of collective beam instabilities in high-energy accelerators* (Wiley, 1993), ISBN 9780471551843, URL <http://www.slac.stanford.edu/~achao/wileybook.html>.
- [33] K. L. Bane and M. Sands, *AIP Conf. Proc.* **367**, 131 (1996).
- [34] A. Piwinski, *DESY-94-068* (1994).
- [35] A. Chao, *AIP Conf. Proc.* **105**, 353 (1983).
- [36] C. Adolphsen et al., *SLAC-R-474*, *LBL-PUB-5424*, *LBNL-PUB-5424*, *UCRL-ID-124161* (1996).

- [37] M. Borland, Advanced Photon Source LS-287 (2000).
- [38] J. Stohr, Tech. Rep. SLAC-I-060-003-000-02-R003, SLAC (2011).
- [39] M. Altarelli et al., Tech. Rep. DESY 2006-097, DESY (2006).
- [40] H. Wiedemann, *Synchrotron Radiation* (Springer, 2003).
- [41] R. Ganter et al., Tech. Rep. PSI Bericht Nr. 10-04, PSI (2010).
- [42] John N. Galayda, Proc. IPAC'18, Vancouver, BC, Canada p. 18 (2018).
- [43] M. Leitner et al., Proc. IPAC'17, Copenhagen, Denmark p. 1605 (2017).
- [44] A. B. Temnykh, Phys. Rev. ST Accel. Beams **11**, 120702 (2008), URL <https://link.aps.org/doi/10.1103/PhysRevSTAB.11.120702>.
- [45] S. Reiche et al., *Genesis User's Manual* (2004), available at <http://genesis.web.psi.ch/>.
- [46] R. Bonifacio, C. Pellegrini, and L. Narducci, Opt. Commun. **50**, 373 (1985).
- [47] Z. Huang and K.-J. Kim, Phys. Rev. ST Accel. Beams **10**, 034801 (2007).
- [48] K. L. F. Bane and G. Stupakov, Conf. Proc. **C0505161**, 3390 (2005), [3390(2005)].
- [49] E.L. Saldin, E.A. Schneidmiller and M.V. Yurkov, *The Physics of Free Electron Lasers* (Springer, Berlin-Heidelberg, 2000).
- [50] P. Schmüser, M. Dohlus and J. Rossbach, *Ultraviolet and Soft X-Ray Free-Electron Lasers* (Springer-Verlag Berlin-Heidelberg, 2008).
- [51] A. Brachmann (2018), ARIES Accelerator Performance and Concept Workshop 2018, Frankfurt am Main, 10–12 December 2018, URL <https://indico.gsi.de/event/7510>.
- [52] J.N. Galayda (2015), Presentation for the U.S. D.O.E. Basic Energy Sciences Advisory Committee.
- [53] I. Robinson, G. Grübel, and S. Mochrie, New Journal of Physics **12**, 035002 (2010).
- [54] E. L. Saldin, E. A. Schneidmiller, and M. V. Yurkov, New Journal of Physics **12**, 035010 (2010), URL <https://doi.org/10.1088%2F1367-2630%2F12%2F3%2F035010>.
- [55] E.L. Saldin, E.A. Schneidmiller, and M.V. Yurkov, Proc. 26th International Free Electron Laser Conference and 11th FEL User Workshop (FEL 04), Conf. Proc. C pp. 139–42 (2004).
- [56] M. Xie, Conf. Proc. C **950501**, 183 (1996).
- [57] R. Bonifacio, N. Piovela, G. R. M. Robb, and A. Schiavi, Phys. Rev. ST Accel. Beams **9**, 090701 (2006), URL <https://link.aps.org/doi/10.1103/PhysRevSTAB.9.090701>.
- [58] C. B. Schroeder, C. Pellegrini, and P. Chen, Phys. Rev. E **64**, 056502 (2001), URL <https://link.aps.org/doi/10.1103/PhysRevE.64.056502>.
- [59] M. Katoh, M. Fujimoto, N. Mirian, et al., **7**, 6130 (2017), URL <https://doi.org/10.1038/s41598-017-06442-2>.
- [60] P. c. v. Rebernik Ribič et al., Phys. Rev. X **7**, 031036 (2017), URL <https://link.aps.org/doi/10.1103/PhysRevX.7.031036>.
- [61] A. Vrieling and N. Sampson, Current Opinion in Structural Biology **13**, 709 (2003), ISSN 0959-440X, URL <http://www.sciencedirect.com/science/article/pii/S0959440X03001702>.
- [62] R. H. Coridan, Ph.D. thesis, University of Illinois at Urbana-Champaign (2009).
- [63] Hilgenfeld, Rolf, the FEBS Journal (2014), URL <https://febs.onlinelibrary.wiley.com/doi/pdf/10.1111/febs.12936>.
- [64] Science and Technology Facilities Council, Tech. Rep., STFC (2016).
- [65] J. Kim, High Pressure Research **36**, 391 (2016).
- [66] F.A. Lima et al., J. Synchrotron Radiation **23**, 1538 (2016).
- [67] B. Marolt (2010), University of Ljubljana, Seminar Note, Ljubljana November 2010.
- [68] J.C. Hemmer et al. (2009), 27-28 October 2008, Rockville, Maryland, U.S.
- [69] M. Yabashi and H. Tanaka, Nature Photonics **11**, 12 (2017).
- [70] V. Petrillo, G. Dattoli, I. Drebot, and F. Nguyen, Phys. Rev. Lett. **117**, 123903 (2016), URL <https://link.aps.org/doi/10.1103/PhysRevLett.117.123903>.
- [71] F. Nguyen, *private communication* (2020).
- [72] F. Nguyen, G. Dattoli, 19th Lomonosov Conference on Elementary Particle Physics, Moscow State University, 22–28 August 2019 (2019).
- [73] T. Ferber, *private communication* (2020).
- [74] K.-J. Kim, Y. Shvyd'ko, and S. Reiche, Phys. Rev. Lett. **100**, 244802 (2008), URL <https://link.aps.org/doi/10.1103/PhysRevLett.100.244802>.
- [75] H. Grote and F. Schmidt, Proc. IEEE PAC 2003, Portland p. 3497 (2000).